

Dynamic Maximization of Oxygen Yield in an Elevated-Pressure Air Separation Unit using Multiple Model Predictive Control

Priyadarshi Mahapatra*, Stephen E. Zitney*, B. Wayne Bequette**

* AVESTAR™ Center, National Energy Technology Laboratory, U.S. Department of Energy, Morgantown, WV 26507, USA
(Tel: 304-285-4063; e-mail: priyadarshi.mahapatra@netl.doe.gov; stephen.zitney@netl.doe.gov).

**Rensselaer Polytechnic Institute, Troy, NY USA (e-mail: bequette@rpi.edu)

Abstract: In a typical air separation unit (ASU) utilizing either a simple gaseous oxygen (GOX) cycle or a pumped liquid oxygen (PLOX) cycle, the flowrate of the liquid nitrogen stream connecting the high- and low-pressure columns has a major impact on the total oxygen yield. It is shown that this yield reaches a maximum at a certain optimal flowrate of LN₂ stream, creating a challenging feedback controller design problem. To dynamically maximize the oxygen yield while the ASU undergoes a load-change and/or a process disturbance, a multiple model predictive control (MMPC) algorithm is proposed. It is shown that at any operating point of the ASU, the MMPC algorithm, through model-weight calculation based on plant measurements, naturally and continuously selects the dominant model(s) corresponding to the current plant state, while making control-move decisions that approach the maximum oxygen yield point. This dynamically facilitates less energy consumption in form of compressed feed-air compared to a simple ratio control during load-swings. In addition, since a linear optimization problem is solved at each time step, the approach involves much less computational cost than a model predictive controller (MPC) based on a first-principles model.

Keywords: Model predictive control, nonlinear systems, process control, air separation unit

1. INTRODUCTION

Cryogenic air separation systems have the capability to deliver the largest capacities for products at a moderate to high-purity level, compared to non-cryogenic based systems such as pressure-swing adsorption (PSA) and membrane technologies, which are typically employed at the lower end of production scale and product purities. The elevated-pressure cryogenic air separation units (ASU) have found application in integrated gasification combined cycle (IGCC) power plants where a typical oxygen molar-purity of 95% is required [1]. Furthermore, in such plants, the high oxygen delivery pressure (~1000 psi) required by the gasifier and the partial integration of an ASU with the combustion turbine, where GT-compressed air is available at high pressures (between 200–250 psi), makes the elevated pressure ASU a promising source of oxygen. Recently, an EP-ASU has been utilized as the primary oxygen source within the Advanced Virtual Energy Simulation Training and Research center at National Energy Technology Center (Morgantown) which features a high-fidelity, real-time dynamic simulator of an IGCC with CO₂ capture process [1]. A typical downside of high-pressure operation is decreased separation efficiency, making the operating cost of such units escalate, in comparison to a low-pressure plant. This cost is by-far compensated with the decreased compressor work during oxygen and nitrogen compression.

It has been shown in previous work [3] that the liquid nitrogen distillate stream from HP-column (stream 'LN₂'), which also serves as a liquid reflux to the LP-column, plays a significant role in the total oxygen yield. In another study by the authors, the MMPC approach was used to capture

dynamic nonlinearities while controlling oxygen purities during rapid ramping operation of the ASU [4]. This operation was done with the abovementioned liquid nitrogen distillate flowrate at either a fixed ratio/feedforward to the oxygen demand or as an augmented feedback loop to the distillate stream nitrogen purity, an approach which is generally utilized by various industries as seen in many patent literatures. This approach closely approaches the optimal yield condition at or near steady state design conditions (assuming the plant is optimally designed at steady state) but does not guarantee an optimal oxygen yield at part-load conditions.

2. STEADY-STATE DESIGN AND DYNAMIC MODEL

The steady-state and dynamic flowsheet design including plant configuration, operating pressures, flowrates, optimization of oxygen recovery, condenser-reboiler heat-integration, "neat" operation and many other intricacies involved in modeling the dynamics of ASU process have been provided in a recent paper by the authors [3]. In addition, some of the interesting problems encountered during operation including refrigeration imbalance and snowball effect within the "cold-box" have also been highlighted. It must be realized by the readers that EP-ASU is a perfect example of process complexity and serves as a good test-bed for various operability and controllability studies. Building the regulatory control layer in this process is, in itself, a daunting task. In fact, numerous patents have been claimed which are centered at developing lower-level controllers in addition to those at PID-based supervisory level control for meeting the stringent load-following requirements posed at deployed sites. Many sources also highlight the

inclusion of a liquid oxygen storage tank for fast load-changes, especially during ramp-up conditions, although

maintaining such a large volumetric space at cryogenic conditions is challenging and capital-cost intensive.

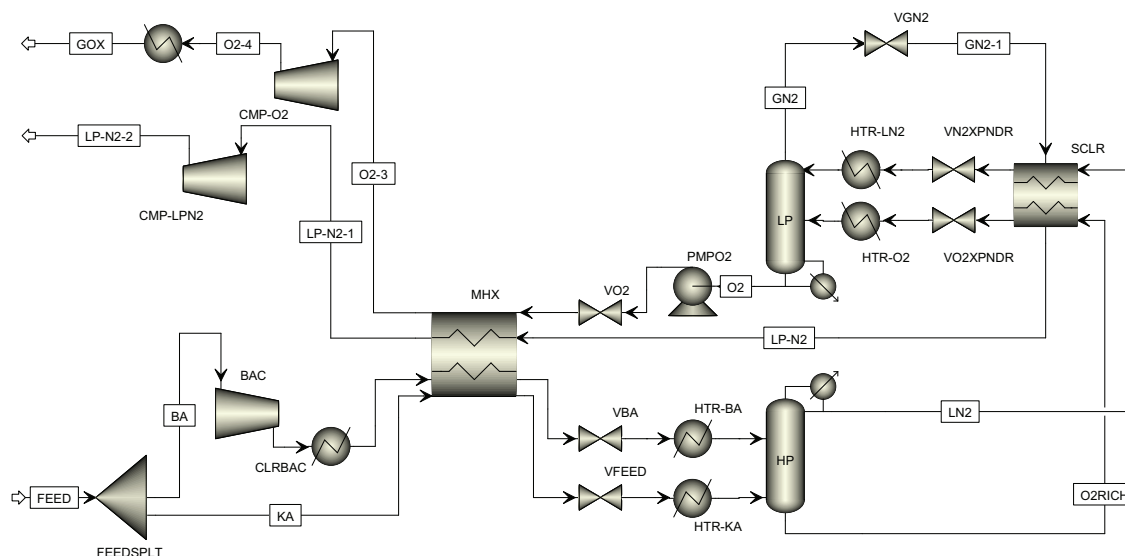


Fig. 1. ASU process flowsheet as seen in Aspen Plus®

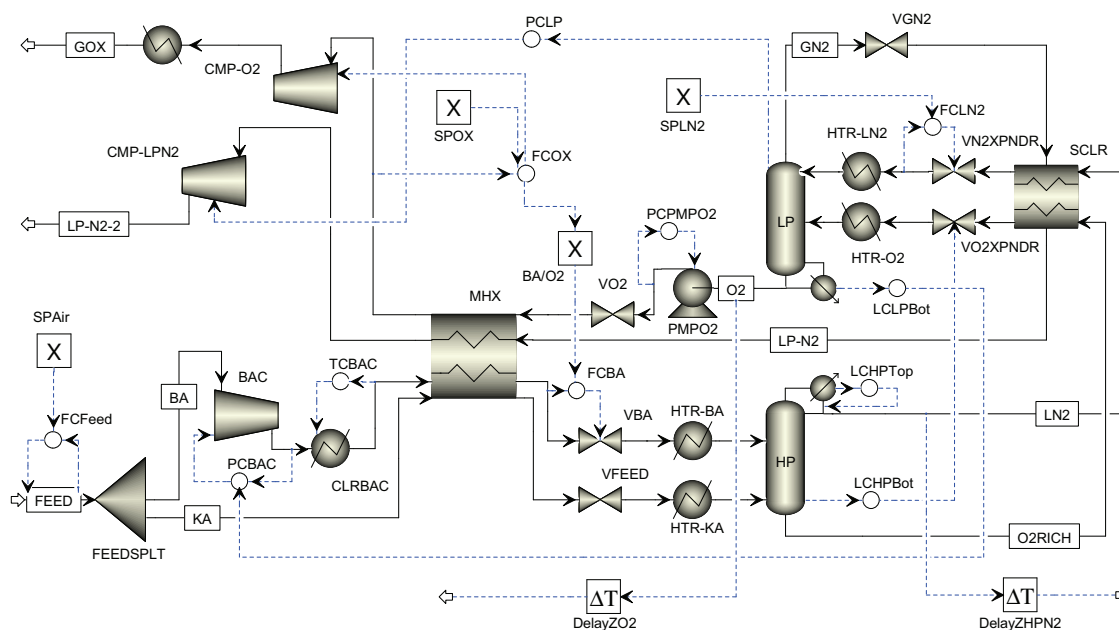


Fig. 2. EP-ASU flowsheet in Aspen Plus Dynamics® showing regulatory controllers and various IO variables exposed for supervisory control layer

A schematic of steady-state flowsheet modeled in Aspen Plus® V7.3 is given in Fig. 1. The dynamic flowsheet modeled in Aspen Plus Dynamics® V7.3 has been shown in Fig. 2. Majority of the steady-state and dynamic flowsheet configurations used in the current study are identical to the previous work by the authors [3]. The only exceptions to such configurations are the absence of supervisory composition control loops in the current design. Instead the input blocks marked by 'SPAir', 'SPLN2' and 'SPOX' are left open. These blocks receive input "setpoint" signals via the Simulink-APD bridge from the MATLAB environment where the supervisory control calculations are being done.

Similarly output signals from the delay blocks ('DelayZO2' and 'DelayHPN2') are being sent to MATLAB as "measured" variables (commonly also known as control variables, CV or process variables, PV).

3. PROBLEM DEFINITION

In general, an efficient plant design takes into account various optimization calculations at the design stage and tries to attain the plant objective in the most effective way. In purview of the EP-ASU for IGCC, the ultimate design objective is to minimize the operating cost of the cold-box. Predominant factors that contribute to the operating cost are

the compression cost of main air compressors (MAC), oxygen and nitrogen compressors. For a given oxygen demand, purity and delivery pressures the operating costs involved in the product-side are do not fluctuate significantly, whereas those on the feed-side i.e. total flowrate of feed-air (and hence the energy consumed in MAC) serves as a good candidate for optimization.

During steady state optimization, rather than minimizing the feed-flow at fixed oxygen purity, an alternate yet equivalent approach is adapted for maximizing the oxygen yield (and hence minimizing the operating costs). This is achieved by maximizing the oxygen purity at a fixed feed-flow. It was identified that liquid-nitrogen stream (Stream 'LN2' in Fig.

1) connecting HP and LP columns, which serves as a distillate for the HP-column and a liquid reflux to the LP-column, has a significant effect on oxygen yield. This has been shown in Fig. 3 (see black curve marked with circles), where a clear maxima is observed at a certain liquid-nitrogen flowrate (~27100 lbmol/hr). On the left hand side (LHS) of this maximum, the oxygen purity gets degraded due to low LP-column reflux leading to lost oxygen in the waste nitrogen stream (Stream 'GN2') whereas on the right hand side (RHS), due to high HP-column distillate extraction, the purification within the HP-column is negatively affected which gets transferred to the overall oxygen separation.

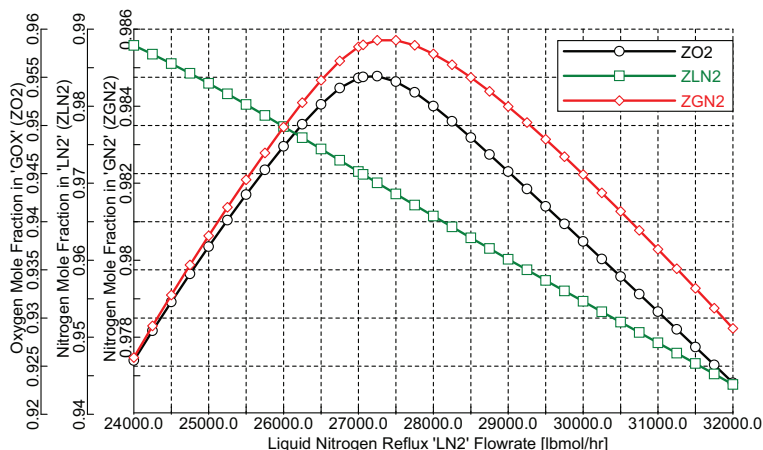


Fig. 3. Sensitivity plots showing effect of liquid-nitrogen reflux 'LN2' flowrate towards oxygen product purity, liquid nitrogen 'LN2' purity and gaseous nitrogen 'GN2' purity at fixed oxygen withdrawal rate (14511.1 lbmol/hr) and total feed air flowrate (69000 lbmol/hr)

In terms of process dynamics, when the system is operated around the optimal flowrate, an input-multiplicity behavior is observed. This is clearly visible in Fig. 4 where 5% step increase and decrease in the 'LN2' flowrate is simulated. Both the open-loop transients settle down to lower oxygen purity values from nominal purity of 0.955. This gives both a negative and positive process gain around the steady-state operating point depending on which direction the process moves. This poses a challenging control problem wherein closed-loop process stability cannot be ensured using a single model / single controller-gain for all possible uncertainties or operating regimes around the nominal operating point.

It can also be seen from Fig. 3 that purity of the abovementioned liquid nitrogen stream denoted by 'ZLN2' monotonically decreases with increasing flowrate ('F_LN2') of the same stream. This is fairly intuitive since with increase in HP-column distillate flowrate, the reflux to this column decreases, leading to a decrease in nitrogen (component having the least molecular wt.) purity. Dynamically this implies that F_LN2 is a strong candidate for controlling ZLN2. This approach has been used by the authors in their previous studies where for a multiloop PID based control, ZLN2 has indeed been tied with F_LN2; and oxygen purity ('ZO2') has been controlled using the total feed air ('F_airASU'). In context of an IGCC power plant, the waste 'gaseous' nitrogen is generally utilized as a gas turbine diluents or as a purge gas during system startup. Hence, meeting the nitrogen purity levels up to a considerable

accuracy is not a strict system requirement. Therefore, various other configurations for multiloop control, where ZLN2 is not actively controlled, were also investigated in search of a control design which would promote faster load-following and/or disturbance rejection. It must be emphasized that in this study the objective is not to control the oxygen and nitrogen purities at nominal values but to dynamically maximize the oxygen yield at the face of a fixed given feed-air flowrate (F_airASU) and oxygen demand (F_O2). As mentioned earlier, this is conceptually equivalent to the case where oxygen purity and demand are kept fixed whereas the feed-air flowrate is minimized (leading to a significant decrease in MAC compression cost). From a problem formulation and implementation perspective, these two cases are dissimilar and scope has been limited to the former in this paper. The following section discusses the multiple model predictive control (MMPC) formulation used for such dynamic maximization of oxygen purity solely based on linear models.

4. MMPPC FORMULATION

The multiple model predictive control strategy [5] is based on the use of n models in the model bank that have the general state-space form given in Eq. (1).

$$\begin{aligned} {}^i\hat{x}_{k|k-1} &= {}^i\Phi {}^i\hat{x}_{k-1|k-1} + {}^i\Gamma^u u_{k-1} + {}^i\Gamma^l l_{k-1} + {}^i\Gamma^d {}^i\hat{d}_{k-1|k-1} \\ {}^i\hat{y}_{k|k-1} &= {}^iC {}^i\hat{x}_{k|k-1} + {}^iD^u u_{k-1} + {}^iD^l l_{k-1} + {}^iD^d {}^i\hat{d}_{k-1|k-1} \end{aligned} \quad (1)$$

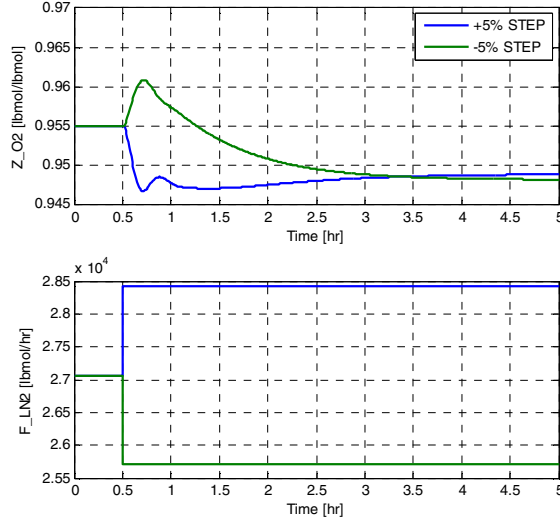


Fig. 4. Transient responses for 5% STEP changes in liquid nitrogen flowrate (F_LN2) for oxygen demand of 14511.1 lbmol/hr and nominal value of F_O2/F_airASU.

where, given the current time step k , the following notations are used:

- u_{k-1} : input (calculated by the controller) between time-step $k-1$ and k
- l_{k-1} : measured and modeled disturbance between time-step $k-1$ and k
- $\hat{d}_{k-1|k-1}$: unmeasured (estimated) but modeled disturbance between time-step $k-1$ and k for model i
- $\hat{x}_{k|k-1}$: process states at time-step k given the plant measurements at time-step $k-1$ (predicted) for model i
- $\hat{x}_{k|k}$: process states at time-step k given the plant measurements at time-step k (corrected) for model i
- $\hat{y}_{k|k-1}$: measured outputs at time-step k given the plant measurements at time-step $k-1$ (predicted) for model i
- $\hat{y}_{k|k}$: measured outputs at time-step k given the plant measurements at time-step k (corrected) for model i

$\Phi, \Gamma^u, \Gamma^l, \Gamma^d, C, D^u, D^l, D^d$ are various state-space parameters for i^{th} model. The left superscript i denotes the model number, with i ranging from 1 to n models. Although the plant being controlled in practice is highly nonlinear (as demonstrated in Fig. 4), the models in Eq.(1) are all linear. Each linear model is chosen to represent a discrete subspace of the overall nonlinear operating space. When all n models are linearly combined, the resulting bank of linear models spans the entire nonlinear operating space. As Fig. 5 shows, the models within the model bank are updated in parallel with the plant.

The state-estimation involves a correction step, which modifies/corrects the plant states based on plant measurements at current time-step. For achieving this, an appended state formulation is used. The following equations list the prediction and correction steps involved in additive-output formulation used in this study.

Prediction Step:

$$\begin{bmatrix} \hat{x}_{k|k-1} \\ \hat{d}_{k|k-1} \end{bmatrix} = \underbrace{\begin{bmatrix} \Phi & 0 \\ 0 & I \end{bmatrix}}_{\Phi^a} \underbrace{\begin{bmatrix} \hat{x}_{k-1|k-1} \\ \hat{d}_{k-1|k-1} \end{bmatrix}}_{\hat{x}_{k-1|k-1}^a} + \underbrace{\begin{bmatrix} \Gamma^u & \Gamma^l \\ 0 & 0 \end{bmatrix}}_{\Gamma^a} \begin{bmatrix} u_{k-1} \\ l_{k-1} \end{bmatrix} \quad (2)$$

$$\hat{y}_{k|k-1} = \underbrace{\begin{bmatrix} C & I \end{bmatrix}}_{C^a} \underbrace{\begin{bmatrix} \hat{x}_{k|k-1} \\ \hat{d}_{k|k-1} \end{bmatrix}}_{\hat{x}_{k|k-1}^a} + \underbrace{\begin{bmatrix} D^u & D^l \end{bmatrix}}_{D^a} \begin{bmatrix} u_{k-1} \\ l_{k-1} \end{bmatrix}$$

Correction Step:

$$\begin{bmatrix} \hat{x}_{k|k} \\ \hat{d}_{k|k} \end{bmatrix} = \begin{bmatrix} \hat{x}_{k|k-1} \\ \hat{d}_{k|k-1} \end{bmatrix} + \underbrace{\begin{bmatrix} 0 \\ I \end{bmatrix}}_{L_k} (y_k - \hat{y}_{k|k-1}) \quad (3)$$

$$\hat{y}_{k|k} = C^a \begin{bmatrix} \hat{x}_{k|k} \\ \hat{d}_{k|k} \end{bmatrix} + D^a \begin{bmatrix} u_{k-1} \\ l_{k-1} \end{bmatrix}$$

The model residuals are calculated as given in Eq. 4 and thereafter the current Bayesian probability ρ_k is calculated recursively using actual-plant output as given in Eq. (5).

$${}^i \varepsilon_k = y_k - \hat{y}_{k|k} \quad (4)$$

$${}^i \rho_k = \frac{\exp\left(-\frac{1}{2} {}^i \varepsilon_k^T {}^i \Lambda {}^i \varepsilon_k\right) {}^i \rho_{k-1}}{\sum_{j=1}^n \exp\left(-\frac{1}{2} {}^j \varepsilon_k^T {}^j \Lambda {}^j \varepsilon_k\right) {}^j \rho_{k-1}}, \quad {}^i \rho_k = \begin{cases} {}^i \rho_k & {}^i \rho_k \geq \delta \\ \delta & {}^i \rho_k < \delta \end{cases} \quad (5)$$

where, ${}^i \Lambda = \begin{bmatrix} {}^i \lambda_1 & & 0 \\ & \ddots & \\ 0 & & {}^i \lambda_{n_y} \end{bmatrix}$ gives the model-residual

covariance matrix. For brevity, each of the diagonal elements is kept identical.

Here, δ represents a small non-zero value used to prevent model-probabilities reaching zero during recursive calculations thereby ensuring that all models remain active during weight-calculations.

The normalized probabilities (model weights) w_k are calculated in Eq. (6) after which the average linear model output vector (\bar{y}) is computed in Eq. (7).

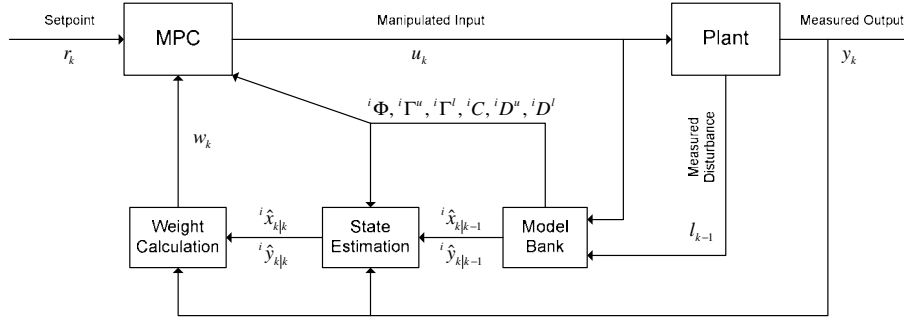


Fig. 5. Block diagram showing the generic multiple model predictive control (MMPC) formulation

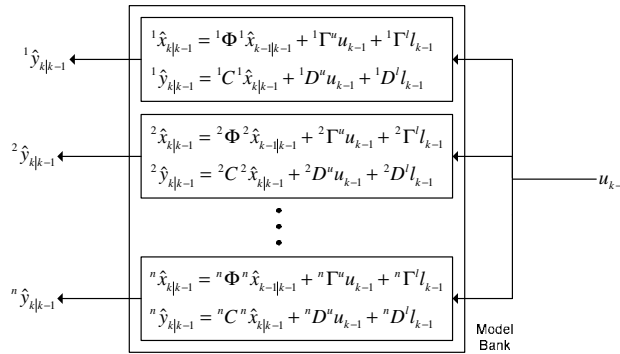


Fig. 6. Schematic showing ‘insides’ of the model bank

$${}^i w_k = \begin{cases} \frac{{}^i \rho_k}{\sum_{j=1}^n {}^j \rho_k} & {}^i \rho_k \geq \delta \\ 0 & {}^i \rho_k < \delta \end{cases} \quad (6)$$

$$\bar{y}_{k+j|k} = \sum_{i=1}^n {}^i w_k {}^i \hat{y}_{k+j|k} \quad (7)$$

This average output vector is used while formulating the constrained MPC objective function (J) as shown in Eq. (8).

$$\min J = \sum_{j=1}^P (r_k - \bar{y}_{k+j|k})^T W^y (r_k - \bar{y}_{k+j|k}) + \sum_{j=0}^{M-1} \Delta u_{k+j}^T W^u \Delta u_{k+j} \quad (8)$$

where, $u_{\min} \leq u_{k+j} \leq u_{\max}$, $\Delta u_{\min} \leq \Delta u_{k+j} \leq \Delta u_{\max}$ and $y_{\min} \leq \bar{y}_{k+j|k} \leq y_{\max}$ are the imposed constraint conditions, r_k is the setpoint vector at current time-step, W_u and W_y are the input and output weighting matrices respectively, P is the prediction horizon and M is the control horizon.

5. SYSTEM IDENTIFICATION

As discussed earlier, flowrate of liquid nitrogen (F_LN2), product oxygen (F_O2) and feed air (F_airASU) play an important role in the oxygen purity (ZO2). Oxygen purity monotonically increases with feed-air flowrate (not shown) and inclusion of this variable in the optimization formulation will only lead to unrealistically high feed-air flowrate giving ultra-high purity oxygen ($ZO2 \approx 1$). Hence, for solving the

current dynamic maximization problem the flowrate of feed-air needs to be fixed with respect to the oxygen flowrate. Here, a fixed ratio of these quantities based on steady-state values has been imposed as given in Eq. (9).

$$\frac{F_{\text{airASU SP}}}{F_{\text{O2 SP}}} = 4.755 \quad (9)$$

where, SP following the variable name denotes the setpoint value sent to the regulatory flow-controllers (signals from supervisory layer) which control the corresponding variable. F_airASU SP and F_O2 SP correspond to signals from ‘SPAir’ and ‘SPOX’ (shown in Fig. 2) respectively.

Before moving to control implementation, the model parameters for all the control-models in the model-bank have to be determined. In essence, the state-space time-invariant matrices $\Phi, \Gamma^u, \Gamma^l, C, D^u, D^l, D^d$ shown in Eq. (1) must be defined for each model.

In this study, two models have been specified. One of them spans the left hand side (LHS) of the maximum point (Fig. 3) and has a positive process gain. In contrast, the other model captures the right hand side (RHS) dynamics and possesses a negative process gain. Starting from the optimal steady-state design conditions, the LHS-model (Model-1) is obtained by first moving to a new operating point on the LHS. This is attained by keeping the oxygen demand (F_O2 SP) unchanged while providing a 10% step decrease in liquid nitrogen (F_LN2 SP).

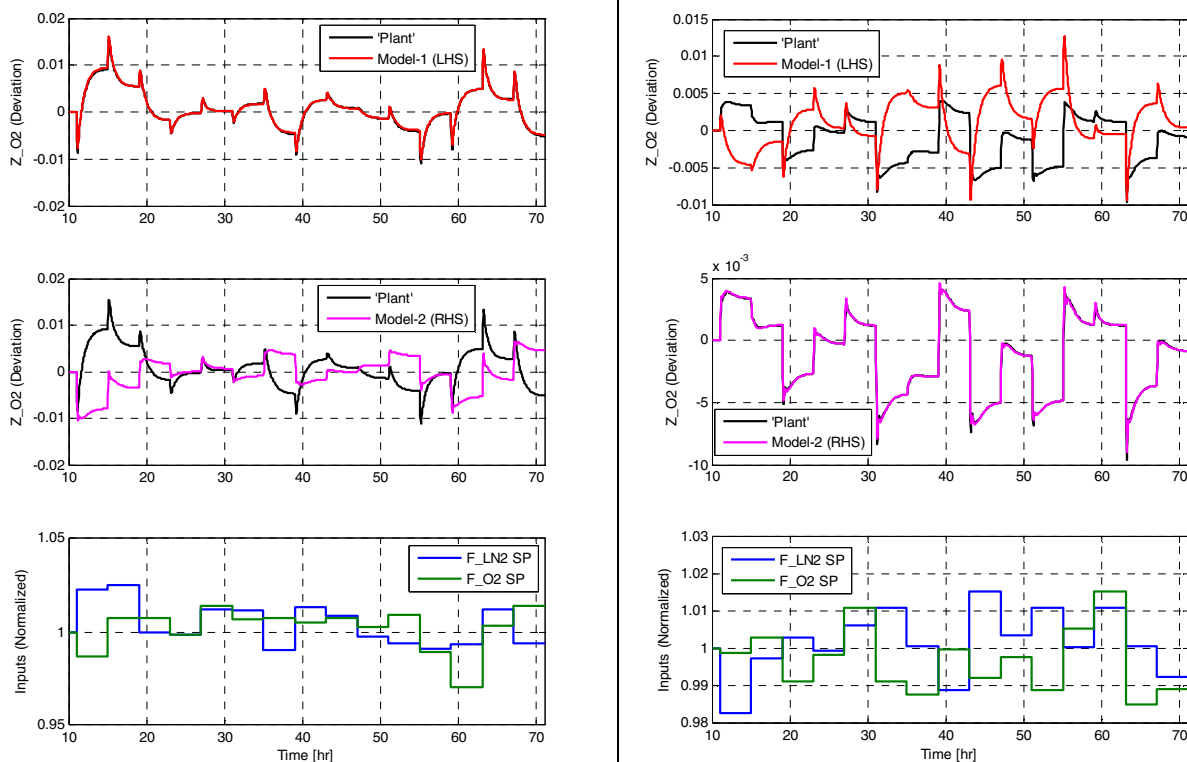


Fig. 7. System Identification results showing quality of fit for Model-1 (left) and Model-2 (right). Input excitations have been shown at the bottom (on each side). Plant outputs are shown in black.

The process is brought to a new steady state by simulating the process for a long time (10 hr). Thereafter, multiple simultaneous random step changes are triggered on both the inputs (F_LN2 SP and F_O2 SP) at regular intervals (until significant settling is observed). The output “plant” signals are fitted to a 4th order subspace-based “n4sid” model (termed as “control-model”) using System Identification Toolbox in MATLABTM. A similar approach is used to obtain the RHS-model (Model-2) as well by providing a 10% step increase in nitrogen flowrate to obtain a new steady state.

Identification (model-fit) results are shown in Fig. 7 for LHS and RHS operating points. The resulting fits show that both the LHS (Model-1) and RHS (Model-2) models capture the plant responses with reasonable accuracy. For comparing and contrasting the behavior of both models, the outputs from the “other” model are also shown (middle plot for LHS and top plot for RHS). It is clearly visible that both models have gains (and even transients) in opposite direction. It must also be noted that the fixed-ratio criterion given in Eq. (9) ensures, to a certain extent, that for all possible combination of input variables the model does not crossover to the other regime. This is consistent with the plots.

6. RESULTS and DISCUSSION

A summary of simulation results obtained for the unconstrained MMPC control design using the two identified models is shown in Fig. 8. Starting with a RHS operating

point ($ZO_2 = 0.95$ and $F_{LN2} = 28260$ lbmol/hr), a pseudo-setpoint of high oxygen-purity value (0.956) is provided. This setpoint can take any value higher than expected maximum oxygen purity. The control algorithm tries to reach this SP by manipulating F_LN2 in a direction adherent to increase in purity but eventually the plant crosses-over to the other regime where further manipulating F_LN2 in the same direction starts bringing down the purity levels. The MMPC algorithm through weighing calculation start prioritizing the “other” model based on decreasing plant purity and the direction of F_LN2 actuation changes. This implies that the plant does not reach the given pseudo-setpoint value (since it is physically not possible to do so for given inlet flowrates), but operates very close to this maximum value. In Fig. 8, the optimal plots for F_LN2 and Z_O2 have been shown. Clearly, the manipulated inputs seem to converge to a point where minor wobbling around optimal point (red-dotted line) can be observed.

7. EXTENSIONS and FUTURE WORK

In the current study, the demand for oxygen (and hence the feed-air) is maintained at a fixed value. In future work, the use of this strategy during load changes including ramp operations will be investigated. It is anticipated that feed-air flowrate will be a better candidate for regulating oxygen purities during fast load changes compared liquid nitrogen flowrate. In addition, if model crossovers occur while the plant is ramping, it might lead to sudden dip in purity level before the MMPC algorithm switches the model.

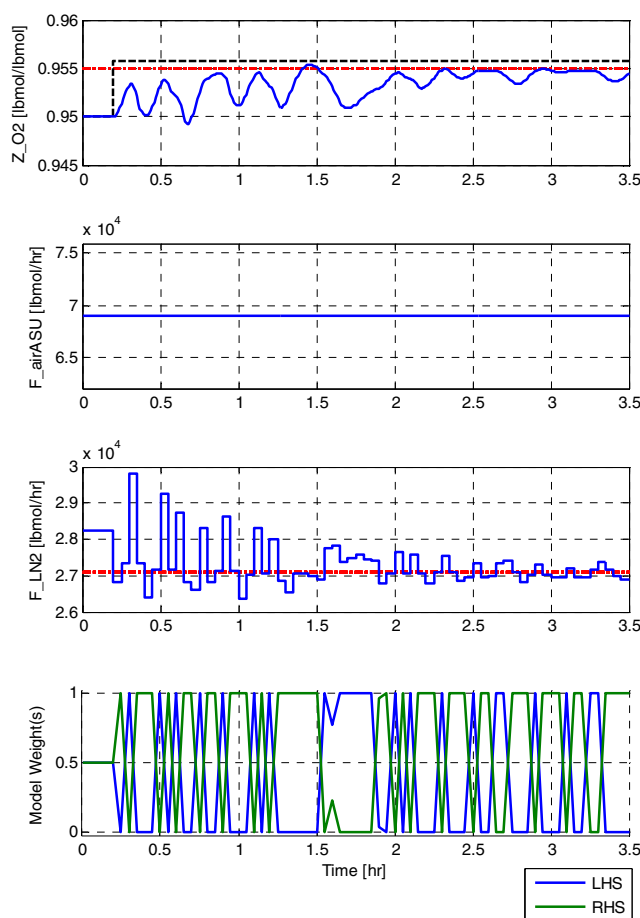


Fig. 8. Simulation results showing dynamic maximization of oxygen purity (Z_{O2}) for fixed oxygen demand (14511.1 lbmol/hr) and feed-air flowrate (69000 lbmol/hr). Optimum operation is shown in dotted-red. Pseudo-SP for oxygen purity is given in dotted-black. MMPC parameters: $P = 100$, $M = 20$, $\lambda_{ii} = 10^8$.

In such situations, a two input (F_{airASU} , F_{LN2}) – two output (Z_{O2} , Z_{LN2}) single-model MPC implementation to meet oxygen purity during fast ramp-changes, should be prioritized. Once the transients settled down, the MMPC algorithm may be triggered for maximizing the purity around the new steady-state.

Another implementation for run-time optimization of the ASU may be done using feed-air flowrate minimization approach (at constant oxygen purity) in contrast to the current approach. Here, constant oscillations in feed-air flowrate may be observed as the liquid nitrogen fluctuates to maximize oxygen purity. Although such dynamic oscillations may at first discourage the implementation of proposed algorithms, it must be realized that over a period of time the difference in required feed-air prevent huge costs involved in expensive air compression.

REFERENCES

- [1] U.S. Department of Energy. Cost and Performance Baseline for Fossil Energy Plants, Volume 1: Bituminous Coal and Natural Gas to Electricity. Technical Report
- [2] S.E. Zitney, E.A. Liese, P. Mahapatra, R. Turton, D. Bhattacharyya, and G. Provost. Advanced Virtual Energy Simulation, Training, and Research: IGCC with CO₂ Capture Power Plant, *Proc. of the 28th Annual International Pittsburgh Coal Conference*, Pittsburgh, PA, September 12-15, 2011.
- [3] P. Mahapatra and B.W. Bequette. Design and Control of an Elevated-Pressure Air Separation Unit for IGCC Power Plants in a Process Simulator Environment, *Industrial & Engineering Chemistry Research*, 52(9), 3178-3191 (2013).
- [4] P. Mahapatra, B.W. Bequette, and S.E. Zitney. Multiple Model Predictive Control of Air Separation Unit as part of IGCC Power Plant during Rapid Load Changes, presented at the 2011 *AIChE Annual Meeting*, Minneapolis, MN, October 16-21, 2011
- [5] M. Kurre-Kinsey and B.W. Bequette. Multiple Model Predictive Control Strategy for Disturbance Rejection, *Industrial & Engineering Chemistry Research*, 49(17): 7983–7989, 2010